Journal of the American College of Cardiology
© 2005 by the American College of Cardiology Foundation
Published by Elsevier Inc.

Vol. 45, No. 8, 2005
ISSN 0735-1097/05/$30.00
doi:10.1016/j.jacc.2004.12.070

Separating Non–Isthmus- From Isthmus-Dependent Atrial Flutter Using Wavefront Variability

Sanjiv M. Narayan, MB, MD, FACC, Alborz Hassankhani, MD, PHD, Gregory K. Feld, MD, FACC, Valmik Bhargava, PHD

San Diego, California

OBJECTIVES The aim of this study was to separate isthmus-dependent atrial flutter (IDAFL) from non–isthmus-dependent atrial flutter (NIDAFL) from the electrocardiogram (ECG) based on functional differences.

BACKGROUND The ECG analyses of F-wave shape suboptimally separate NIDAFL from IDAFL. The authors hypothesized that anatomic and functional differences may result in greater wavefront variability in NIDAFL than IDAFL, allowing their separation. The authors tested this hypothesis in patients undergoing ablation for atrial flutter using a novel ECG algorithm to detect subtle F-wave variability, validated by intracardiac measurements.

METHODS In 62 patients (23 NIDAFL, 39 IDAFL) ECG atrial wavefronts were represented as correlations of an F-wave template to the ECG over time. Correlations in orthogonal ECG lead-pairs were plotted at each time point to yield loops reflecting temporal and spatial regularity in each plane. The ECG analyses were compared with intracardiac standard deviations of: 1) atrial electrograms (temporal variability), and 2) bi-atrial activation time differences (spatial variability).

RESULTS Atrial ECG temporospatial loops were reproducible in IDAFL, but varied in NIDAFL ($p < 0.01$) suggesting greater variability that correctly classified IDAFL (39 of 39 cases) from NIDAFL (22 of 23 cases; $p < 0.001$). Intra-atrial mapping confirmed greater temporal variability for NIDAFL versus IDAFL, in lateral ($p < 0.01$) and septal ($p = 0.03$) right atrium, and proximal ($p = 0.02$) and distal ($p < 0.01$) coronary sinus. Spatial variability was greater in NIDAFL than IDAFL ($p = 0.02$).

CONCLUSIONS Greater cycle-to-cycle atrial wavefront variability separates NIDAFL from IDAFL and is detectable from the ECG using temporospatial analyses. These results have implications for guiding ablation and support the concept that IDAFL and NIDAFL lie along a spectrum of intracardiac organization. (J Am Coll Cardiol 2005;45:1269–79) © 2005 by the American College of Cardiology Foundation

Classifying atrial macro–re-entry from the electrocardiogram (ECG) is central in guiding the approach to ablation yet remains suboptimal. Typical atrial flutter is defined by atrial waveforms that are inverted in the inferior ECG leads and upright in lead V_1 (1) (sub-eustachian isthmus-dependent atrial flutter [IDAFL], counterclockwise [CCW]), or "inverted" in reverse typical atrial flutter (clockwise [CW]) (2). However, such F waves are also seen in atypical atrial macro–re-entry (non–isthmus-dependent atrial flutter [NIDAFL]) (3,4), including left atrial circuits (5). Furthermore, F waves in IDAFL may be "atypical" in patients with atrial enlargement, heart failure, factors favoring atrial fibrillation (6), or varying bi-atrial activation (7,8). These observations may explain why the absence of typical F waves does not accurately separate NIDAFL from IDAFL (2).

We hypothesized that functional differences may separate forms of stable atrial flutter. Although it is increasingly felt that IDAFL and NIDAFL lie along an organizational spectrum that interfaces with atrial fibrillation (2,9), this suggests either that NIDAFL is less organized than IDAFL or simply less stereotypical. However, these concepts may be interrelated. Certainly, macro–re-entry in IDAFL is stereotypical, yet it also occupies a large portion of the right atrium and is bounded significantly by anatomic obstacles so that passive activation of right and left (10) atria are also stereotypical, and cycle-to-cycle variability is limited. Conversely, the variable location of circuits in NIDAFL relative to anatomic obstacles, and smaller zones of conduction block (or scar), may render passive activation more susceptible to functional block and allow greater cycle-to-cycle variability. Although reports hint at greater F-wave variability in stable NIDAFL than IDAFL (5,11,12), this difference has not been quantified and is not used routinely to separate NIDAFL from IDAFL (2).

We tested the hypothesis that subtle F-wave variability between cycles would distinguish NIDAFL from IDAFL, by developing a sensitive ECG algorithm (13) then validating our findings from detailed clinical mapping in patients undergoing ablation of atrial arrhythmias.

From the University of California and Veterans Administration Medical Centers, San Diego, California. This study was supported by a grant from the National Heart, Lung and Blood Institute to Dr. Narayan (HL 70529). Fred Morady, MD, acted as Guest Editor for this paper.

Manuscript received October 4, 2004; revised manuscript received December 6, 2004; accepted December 7, 2004.

JACC Vol. 45, No. 8, 2005
April 19, 2005:1269–79

Abbreviations and Acronyms

A:V = atrio:ventricular
CCW = counter-clockwise
CL = cycle length
CS = coronary sinus
CW = clockwise
ECG = electrocardiogram
EPS = electrophysiologic study
FFT = Fast Fourier Transform
IDAFL = isthmus-dependent atrial flutter
LA = left atrium
NIDAFL = non–isthmus-dependent atrial flutter
IVC = inferior vena cava
RA = right atrium
TA = tricuspid annulus

METHODS

Clinical protocol. We studied 62 consecutive patients referred to the University of California (UCSD) and Veterans' Affairs Medical Centers (VAMC), San Diego, for electrophysiologic study (EPS) and ablation of stable atrial macro–re-entry, defined from prior ECGs and subsequently using entrainment. This study was approved by the joint UCSD/VAMC Institutional Review Board. Patients were excluded if they were too unstable to undergo EPS or were inadequately anticoagulated, unless they lacked atrial thrombus on transesophageal echocardiography.

Patients underwent EPS in the fasting state after discontinuing anti-arrhythmic and rate control medications (Table 1). Catheters were advanced transvenously to the His bundle position (quadrapolar) and coronary sinus (CS) (decapolar). A duodecapolar ("Halo") catheter was placed in the right atrium (RA) parallel to the tricuspid annulus (TA) with its proximal poles at the inter-atrial septum and its distal poles across the inferior vena cava (IVC)-TA isthmus. An ablation catheter (EP technologies, Sunnyvale, California) was used for mapping.

Table 1. Clinical Characteristics

	IDAFL (n = 39)	NIDAFL (n = 23)	p Value
Age (yrs)	58.5 ± 13.5	60.6 ± 12.8	NS
AFL CL (ms)	246.7 ± 30.8	291.2 ± 42.2	< 0.01
Ventricular CL (ms)	617.7 ± 200.6	685.3 ± 215.3	NS
Atrio:ventricular ratio	2.5 ± 0.8	2.4 ± 0.8	NS
LA diameter (mm)	38.9 ± 9.2	43.7 ± 7.8	NS
LVEF (%)	58.0 ± 16.5	51.3 ± 12.2	NS
NYHA heart failure class ≥II	0	3	NS
Prior cardiac surgery	6	11	< 0.01
Medications			
Anti-arrhythmic*	22	9	NS
Rate-slowing†	25	10	NS
Hypertension	18	8	NS
Diabetes mellitus	7	3	NS

*Prior therapy with class I or class III agents; †therapy with beta-blocker or calcium antagonists.

AFL = atrial flutter; CL = cycle length; IDAFL = isthmus-dependent atrial flutter; LA = left atrial; LVEF = left ventricular ejection fraction; NIDAFL = non–isthmus-dependent atrial flutter; NYHA = New York Heart Association.

Isthmus-dependent atrial flutter was diagnosed by sequential (CCW or CW) activation around the TA, concealed entrainment at the IVC-TA isthmus, and the inability to reinduce atrial flutter after creating bidirectional block across the IVC-TA isthmus by drag-line ablation. Non–isthmus-dependent atrial flutter was diagnosed by a distinct activation pattern from IDAFL, concealed entrainment at sites of earliest atrial activation or double potentials outside the IVC-TA isthmus, and termination and the inability to reinduce after ablation at these sites. An electroanatomic mapping system (Carto, Biosense-Webster, Diamond Bar, California) was used in NIDAFL to help localize the critical earliest site of activation and the isthmus of macro–re-entry for ablation (16 of 23 cases).

Acquisition of data. We recorded 12-lead surface ECGs (filtered at 0.05 to 100 Hz) and simultaneous bipolar intracardiac electrograms (30 to 100 Hz) of atrial flutter, digitized at 1 kHz to 16-bit resolution (Bard, Billerica, Massachusetts).

Analyses were blinded to all clinical data. Electrograms were analyzed on a personal computer using software written by the authors (S.M.N.) in Labview (National Instruments, Texas) (13). The ECG analysis focused on leads V_5, aVF, and V_1, related to orthogonal leads X, Y, and Z, respectively. Intracardiac electrograms were analyzed at 200 mm/s scale.

ECG temporal regularity. Analyses were blinded to clinical and EPS data. We quantified F-wave temporal and spatial variability as recently described (13). Briefly, ECG F-waves were represented by a 120-ms sample selected to avoid isoelectric ECG segments (Fig. 1). Each sample was cross-correlated to its ECG at successive time points using the Pearson coefficient on M pairs of data (A_{k+i}, B_{j+i}), where A_{k+i} and B_{j+i} are corresponding points of the F-wave sample and native ECG:

$$r_j = \frac{M\left(\sum_{i=1}^{M} A_{k+i}B_{j+i}\right) - \sum_{i=1}^{M} A_{k+i}\sum_{i=1}^{M} B_{j+i}}{\sqrt{\left[M\sum_{i=1}^{M} A_{k+i}^2 - \left(\sum_{i=1}^{M} A_{k+i}\right)^2\right]\left[M\sum_{i=1}^{M} B_{j+i}^2 - \left(\sum_{i=1}^{M} B_{j+i}\right)^2\right]}}$$

where r_j is the coefficient at the *jth* timepoint; j ranges from the first ECG point to Q − M, ($0 \le j \le$ Q − M), Q being the last ECG point; k ranges from L to L + M ($0 \le L \le$ Q − M). Repeating this operation for all ECG time points results in correlation-time series (Figs. 1, 2A, and 2B, lower left panels), in which F-waves (and the sampled region) have correlation r = 1, whereas non-exact matches (QRS, T-waves) give r values between −1 and +1. Because the correlation approach reduces differences in signal amplitude through scaling, the use of staggered overlapping ECG samples "extracts" F-wave components that are superimposed or partially revealed during a QRS complex or T-wave.

Regularity in F-wave timing was quantified using Fast Fourier Transforms (FFT) of 8.192 s (2^{13} ms) of correlation-

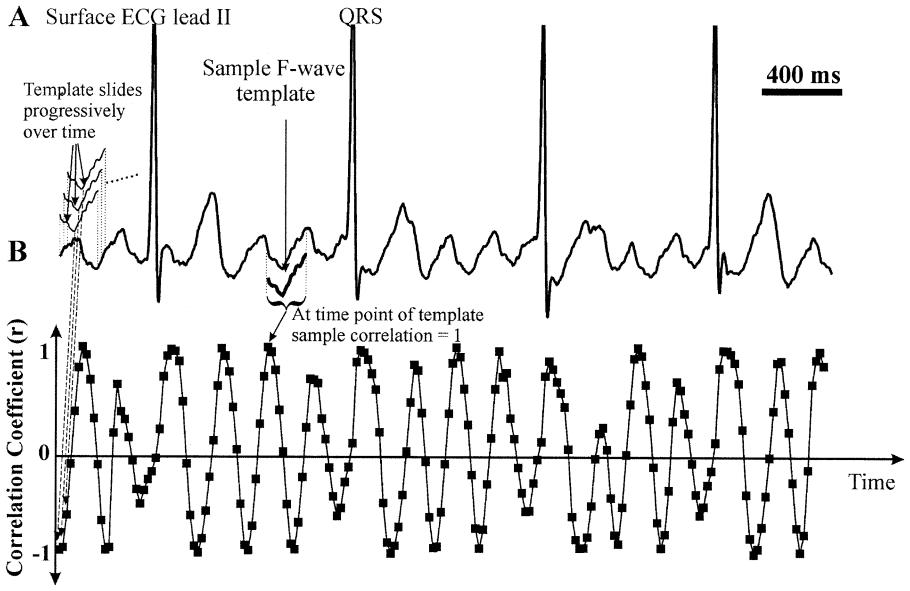

Figure 1. Derived ("filtered") atrial waveforms. **(A)** Electrocardiogram (ECG) shows isthmus-dependent atrial flutter with labeled F-wave sample. **(B)** Correlation of this sample to successive ECG time points produces a correlation time series that reflects "filtered" atrial activity. Peaks ($r \approx 1$) identify F-waves even when partly overlying QRS/T waves.

time series (Figs. 2A and 2B, right panels). We defined temporal (spectral) regularity as a dominant peak magnitude ≥6 dB relative to the subharmonic and harmonic either side and bandwidth ≤8 Hz.

ECG temporospatial regularity. We quantified spatial phase, or the continuous atrial vector during (intracycle) and between (intercycle) successive cycles in each plane. In the XY plane, spatial phase was computed by plotting X- versus Y-axis correlations (leads V_5 versus aVF) at each time point (Fig. 3), similarly for YZ (aVF/V_1) and XZ (V_5/V_1) planes. This resulted in loops for successive cycles that represent temporospatial regularity (Fig. 3A). Although loops may reflect atrial and ventricular activity (resulting from the slight differences in correlation plots seen in Fig. 1), each are independent and thus unaffected by varying atrio to ventricular conduction ratios (Fig. 4A).

When atrial wavefronts maintain spatial vectors between cycles, plots should co-vary between axes at each time point. Successive atrial loops may thus approach (1,1), indicating that F-waves recur simultaneously in both axes (intercycle regularity) (Figs. 3A, 4A, and 4C). Furthermore, the principal axes of atrial loops may lie along X = Y, indicating that atrial activity co-varies between axes throughout the cycle (intracycle regularity) (Figs. 3A, 4A, and 4C). We applied the term *temporospatial coherence* if the upper right turnaround point of each atrial loop passed (0.75, 0.75) in each plane (Fig. 3A). In 3-axes, this requires a distance from the origin $R \geq \sqrt{(0.75^2 + 0.75^2 + 0.75^2)}$; i.e., $R \geq 1.30$. For loop reproducibility, we required standard deviation (SD) of $R \leq 0.15$ (13).

Analyzing intra-atrial temporal and spatial regularity. We compared ECG F-wave variability to the SDs of simultaneous, precisely measured cycle lengths (CL) of 8 to 10 cycles from electrograms at low lateral RA (Halo 3/2), septal RA (Halo 8/9), and proximal and distal CS. Intervals were excluded if electrograms were noisy or contaminated by ventricular activity. Similarly, we measured intra-atrial spatial variability as SDs of bi-atrial activation time differences (8 to 10 cycles), from Halo 3 (or 2) to distal CS bipolar electrograms.

Statistical analyses. Continuous data are presented as mean ± SD. The two-tailed *t* test was used to compare continuous variables between groups. The chi-square test was applied to contingency tables. A probability below 5% was considered significant.

RESULTS

We studied 39 patients with IDAFL (35 CCW, 4 CW) and 23 with NIDAFL. Prior cardiac surgery was more common in patients with NIDAFL than IDAFL (11 of 23 vs. 6 of 39; $p < 0.01$), but groups were otherwise similar (Table 1). Macro–re-entry was confirmed in each case using entrainment with concealed fusion (Fig. 4B) and successfully ablated. Atypical macro–re-entry (NIDAFL) was present at lateral RA scar (n = 8; ablated at lateral RA), crista terminalis (n = 4; ablated via drag lines to vena cavae), lower loop re-entry (n = 2; ablated at isthmus), other RA sites (n = 5), left atrium (LA; n = 3; ablated at mitral isthmus and fossa ovalis), and CS (n = 1).

Similar spectra between IDAFL and NIDAFL. The CLs were shorter for IDAFL than NIDAFL (shortest CL 200 vs. 236 ms; mean 246.7 ± 30.8 ms vs. 291.2 ± 42.2 ms, respectively; $p < 0.01$).

Both IDAFL and NIDAFL showed regularity on FFT spectra. In IDAFL, correlation series (Fig. 2A) show dominant peak magnitude 10.53 dB reflecting the frequency of macro–re-entry. Similar results were seen for all cases of

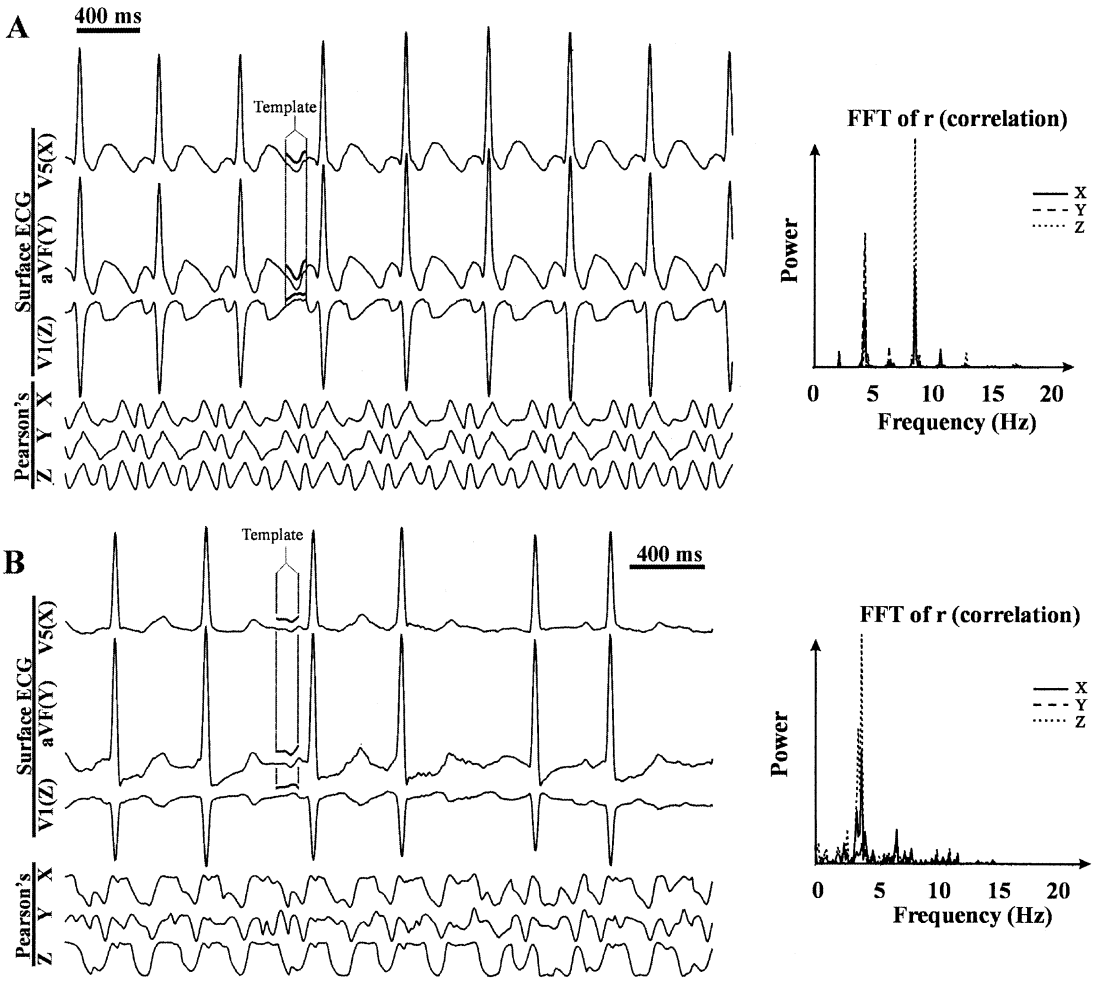

Figure 2. Temporal phase. **(A)** isthmus-dependent atrial flutter shows electrocardiogram (ECG) and correlations of labeled template to ECG, producing regular correlation time series. Peaks where $r \approx 1$ identify recurrent F waves even if superimposed on QRS activity. Power (Fast Fourier Transform [FFT]) spectrum from correlation series shows atrial peak (10.53 dB) at 3.78 Hz. **(B)** Non–isthmus-dependent atrial flutter. Shows ECG with F waves that have some "typical" features but vary. Correlation time series show irregularity. Spectra show one atrial peak (16.72 dB) at 3.42 Hz. Non–isthmus-dependent atrial flutter was confirmed near a right atrial scar and ablated.

IDAFL (Table 2) including CW-IDAFL (e.g., Fig. 4C). Non–isthmus-dependent atrial flutter (Fig. 2B) also showed regularity with a dominant 16.72-dB spectral peak. This case involved macro–re-entry around a right atriotomy scar that was ablated by drag-lesions to the superior vena cava. Similar results were seen for the patient population with NIDAFL (Table 2).

ECG temporospatial regularity of IDAFL versus NIDAFL. Notably, although ECG atrial loops (reflecting temporospatial regularity) were reproducible in 39 of 39 cases of IDAFL, they were reproducible in only 1 of 23 cases of NIDAFL ($p < 0.01$; Table 2), suggesting wavefront variability between cycles of NIDAFL. The ECG temporospatial coherence therefore correctly classified IDAFL and 22 of 23 cases of NIDAFL ($p < 0.001$) despite the fact that several cases of NIDAFL showed F waves closely resembling IDAFL (Figs. 4D to 4F).

Figure 3A shows loops representing atrial cycles for the case of CCW-IDAFL in Figure 2A. Loops approach (1,1) in each plane (intercycle regularity) and are reproducible with principal axes approximating a line joining (0,0) to (1,1) (intracycle regularity). For three axes, $R = 1.51 \pm 0.03$, showing temporospatial coherence. All cases of CW-IDAFL also showed coherent loops ($n = 4$; Fig. 4C).

In contrast, NIDAFL exhibited greater spatial variability. In Figure 3B (same patient as Fig. 2B), only a minority of atrial loops approach (1,1), and loops are neither reproducible nor parallel to lines of identity. For all axes, $R = 0.92 \pm 0.08$ (not coherent). Lack of coherence typified patients with NIDAFL (Table 2). Notably, even when NIDAFL had F waves that were visibly regular, or that resembled "typical" F waves using traditional criteria (2), their loops still exhibited temporospatial variability (Figs. 4D and 4F).

Intracardiac validation of temporal and spatial irregularity of NIDAFL versus IDAFL. Intracardiac measurements and electroanatomic maps (Fig. 4E) confirmed that NIDAFL and IDAFL were stable, regular macro–reentrant circuits. However, measurements also confirmed greater wavefront variability in NIDAFL than IDAFL

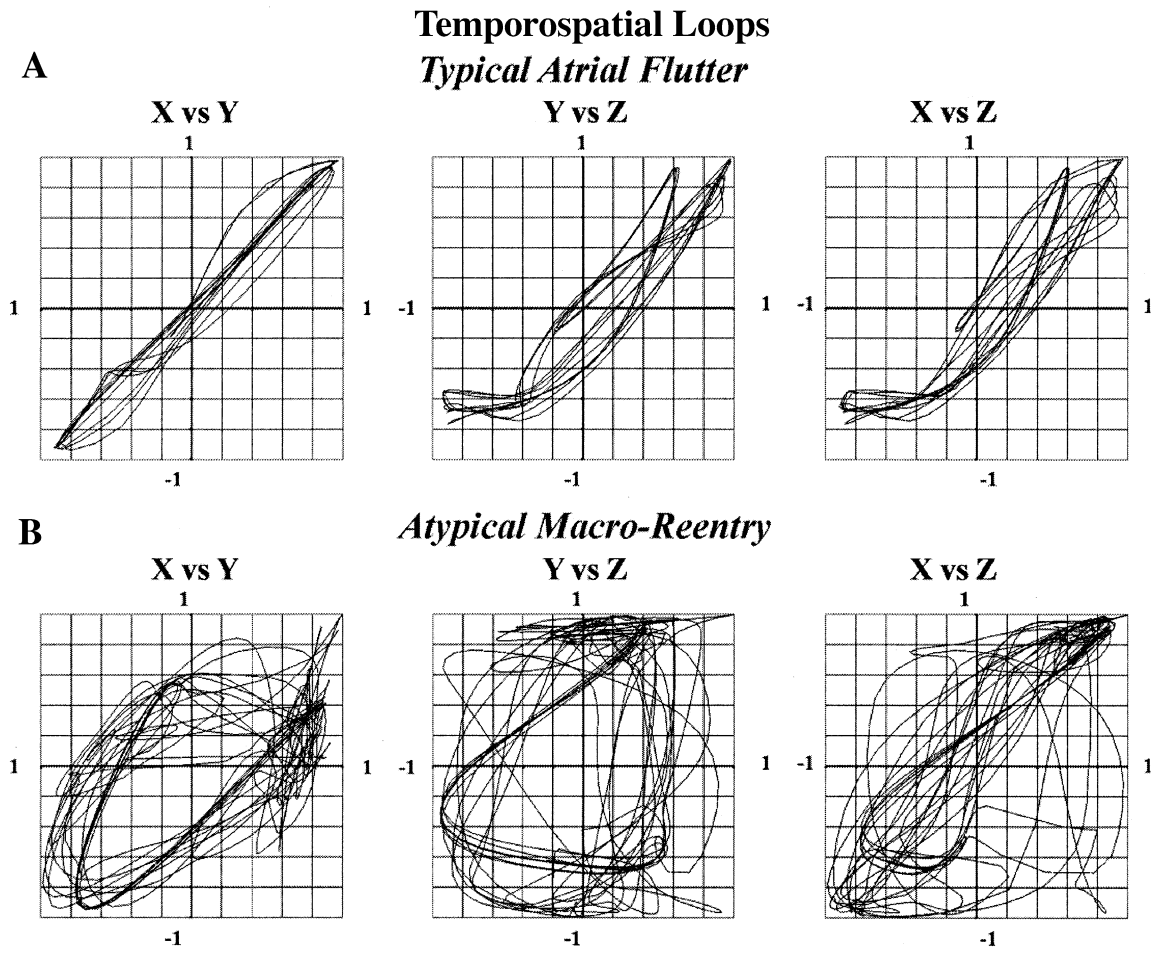

Figure 3. Inter- and intracycle atrial temporospatial loops. Plotting correlation ('r') values each time point between axes yields XY, YZ, and XZ atrial and ventricular loops. **(A)** Isthmus-dependent atrial flutter. Atrial loops approach the (1,1) coordinate, are reproducible, and have excursion from origin, R = 1.51 ± 0.03 (i.e., spatially coherent). **(B)** Non–isthmus-dependent atrial flutter. Loops do not approach (1,1) (R = 0.92 ± 0.08) and are irreproducible, showing atrial wavefront variability amplified by this analysis.

(Table 2), both temporally (SD 7.32 ± 3.03 ms vs. 4.44 ± 2.31 ms for 10 cycles at low RA; $p < 0.01$) and spatially (SD of bi-atrial activation time differences: 4.99 ± 2.21 ms vs. 3.62 ± 2.01 ms; $p = 0.02$).

Figure 5A illustrates intra-atrial recordings in CCW-IDAFL (same patient as Figs. 2A and 3A). Temporally, SD of cycles ranged from 3.32 to 4.58 ms (between RA and LA sites). Spatially, cycles had an SD of bi-atrial activation time difference of 3.32 ms. In contrast, Figure 5B shows that NIDAFL (same patient as Figs. 2B and 3B) showed greater variability in atrial timing, with SD ranging from 5.46 to 8.47 ms, and spatial variability (SD of Halo to CS bi-atrial activation time differences) of 10.15 ms.

DISCUSSION

We show that NIDAFL shows subtle cycle-to-cycle F-wave variability that is greater than IDAFL, allowing ECG separation of these rhythms even when F waves in NIDAFL appeared typical. Moreover, this phenomenon reflects corresponding differences in the variability of intracardiac timing and activation sequence between these rhythms. Although prior studies have hinted at substantial wavefront variability in NIDAFL, the observed differences are robust enough to support the concept that IDAFL and NIDAFL lie along a spectrum of intra-atrial organization and provide a basis for future studies on the transition of atrial flutter to atrial fibrillation.

Greater activation variability in NIDAFL than IDAFL. We show that temporospatial ECG detection of millisecond variability in timing separate NIDAFL from IDAFL, just as microvolt-level alternations in the ECG T-wave (14) and millisecond-level changes in signal averaged P and QRS durations (15) also provide unique clinical information.

In IDAFL, our measured cycle SDs agree closely with those of prior studies (e.g., SD 4.9 ± 1.7 ms [16]). Conversely, NIDAFL showed greater CL SD and inconsistent temporospatial atrial loops whether F-waves were visually regular (Figs. 4D to 4F) or varying (Fig. 2B), suggesting wavefront variability. Variability likely reflects passive (global) atrial activation, reflected by activation sequence variability, rather than in the re-entrant circuit

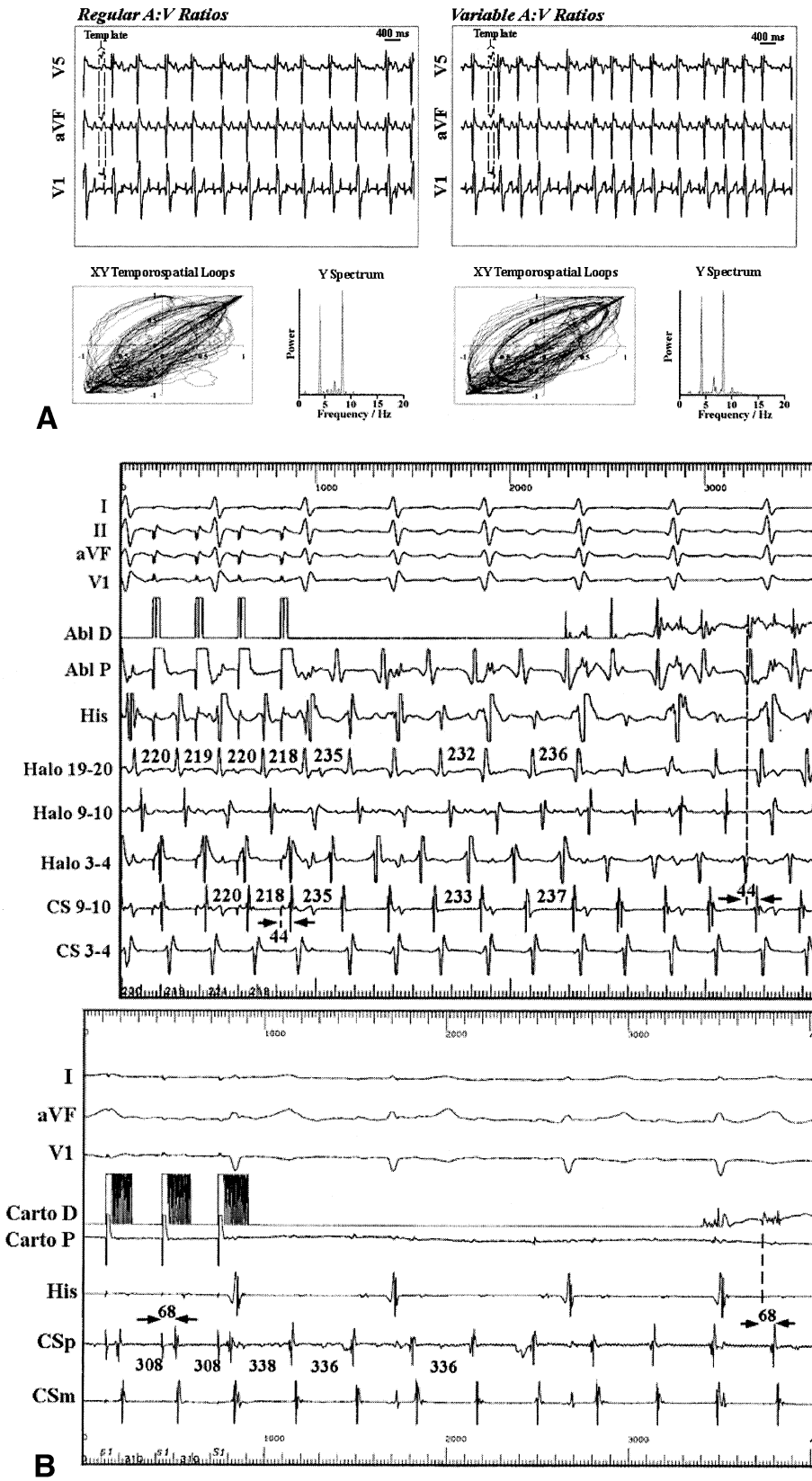

Figure 4. (A) Spatiotemporal loops are unaffected by atrio:ventricular (A:V) ratio, illustrated by here by isthmus-dependent atrial flutter (IDAFL) with regular and variable A:V conduction in the same patient. Loops from each electrocardiogram (ECG) segment reach (1,1) and lie along the line of identity, and spectra are analogous. **(B)** Concealed entrainment in IDAFL **(top)** and non–isthmus-dependent atrial flutter (NIDAFL), show F-wave and electrogram similarity between pacing and tachycardia, post-pacing interval equal to atrial flutter cycle length (CL), and stimulus-electrogram equal to electrogram-electrogram intervals. CS 9–10, CSp = proximal coronary sinus; CS 3–4, CSM = mid-coronary sinus. *Continued on next page.*

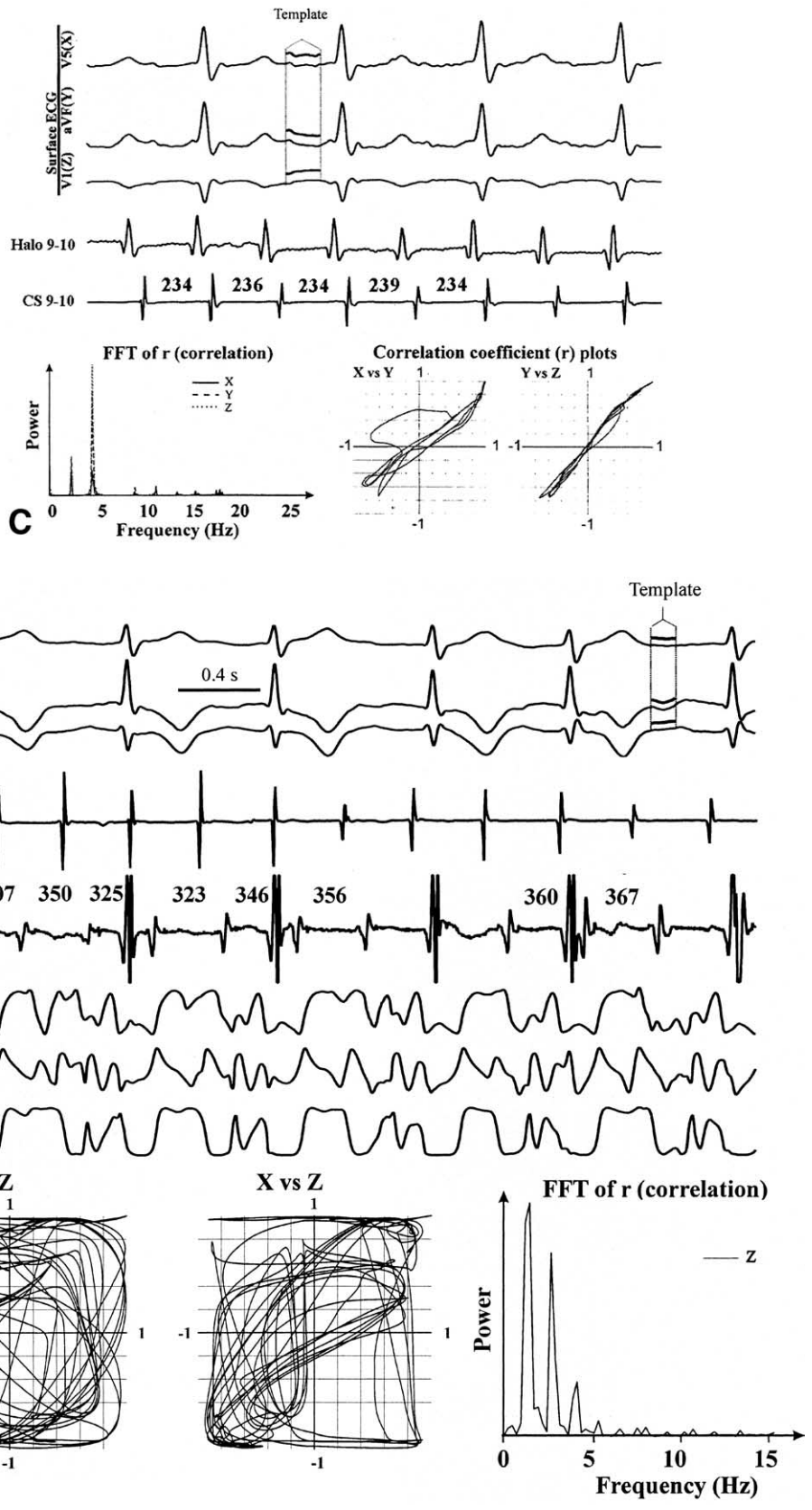

Figure 4 Continued. **(C)** Clockwise IDAFL, shows a dominant spectral peak (14.01 dB) and consistent loops (R = 1.42 ± 0.11; XY, YZ shown). **(D)** NIDAFL with variable ECG spatial loops and marked intracardiac CL variability; ablated in low lateral right atrium. CS-D = distal coronary sinus; RF = mapping catheter. *Continued on next page.*

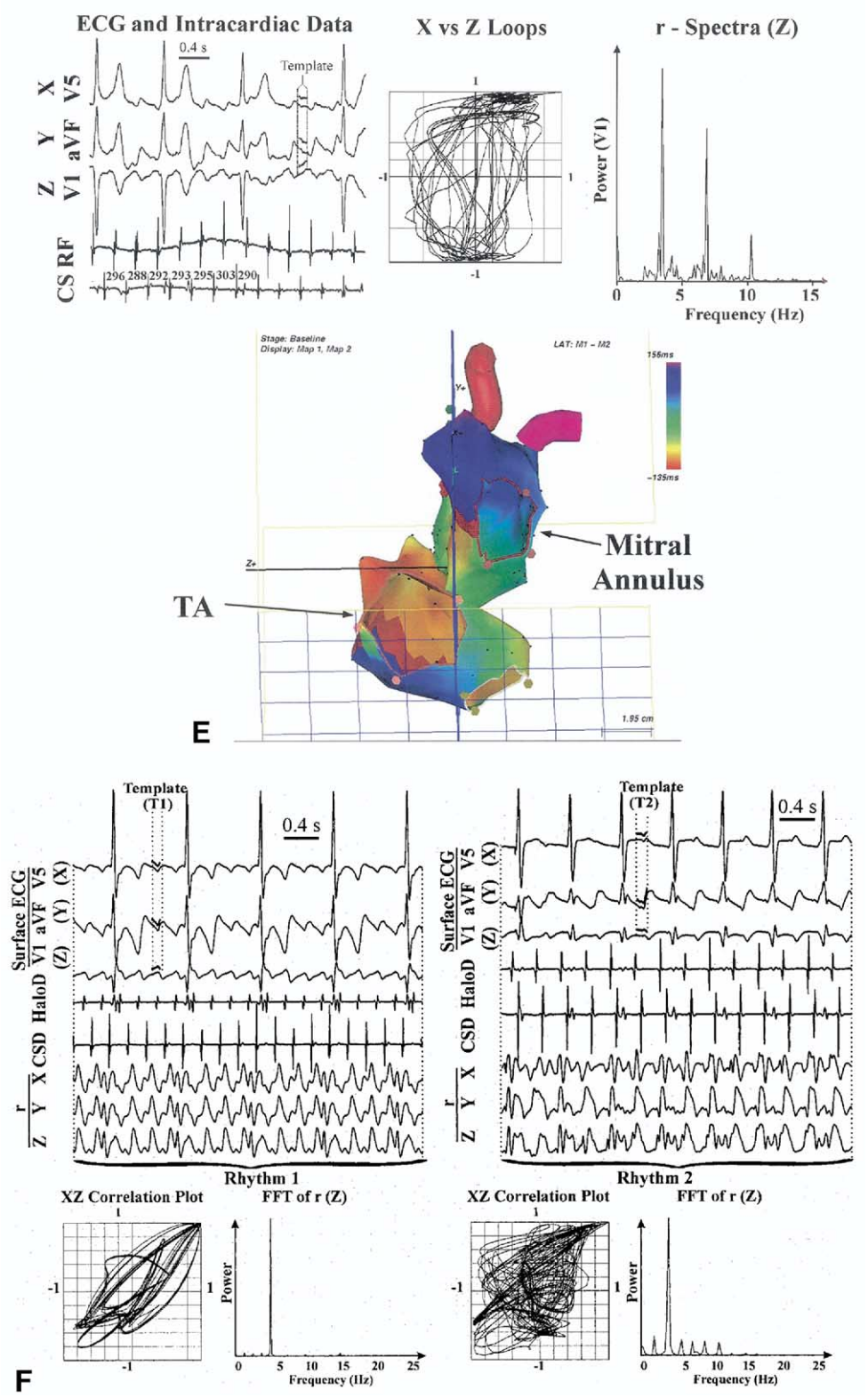

Figure 4 Continued. **(E)** Counterclockwise mitral annulus NIDAFL. The ECG was interpreted as NIDAFL or atrial fibrillation. Dominant spectral peak (8.91 dB) yet variable loops (R = 0.94 ± 0.13) suggested NIDAFL. Bi-atrial electroanatomic maps showed counterclockwise re-entry around the mitral annulus, with passive counterclockwise tricuspid annulus (TA) activation (left anterior oblique projection), that was entrained then ablated from left lower pulmonary vein to mitral annulus. Standard deviation of CL was 9.9 ms (distal CS) and 13.5 ms (low lateral right atrial). **(F)** Similar ECGs but dissimilar atrial flutter mechanisms. **(Left)** Dominant peak (19.44 dB) and consistent loops (R = 1.56 ± 0.02) confirmed counterclockwise IDAFL; TA-inferior vena cava isthmus ablation caused bidirectional block. **(Right)** Separately induced atrial flutter looked similar on ECG, yet varying loops (R = 1.11 ± 0.11) suggested NIDAFL. Macro–re-entry was entrained in the lateral right atrium and ablated using drag-line to superior vena cava. CS = coronary sinus; FFT = Fast Fourier Transform; RF = mapping catheter.

Table 2. ECG and Intracardiac Temporal and Spatial Regularity

	IDAFL (n = 39)	NIDAFL (n = 23)	p Value
ECG temporal regularity (spectra)			
Spectral peak on r-series ≥6dB	39	22	NS
ECG temporospatial regularity (loops)			
Spatial phase magnitude: *R*	1.44 ± 0.07	1.09 ± 0.18	< 0.01
Number of patients with *R* mean ≥1.30 and *R* SD ≤ 0.15	39	1	< 0.01
Intracardiac temporal regularity (SD of atrial CL/ms)			
At low RA	4.44 ± 2.31	7.32 ± 3.03	< 0.01
At septal RA	4.27 ± 2.68	7.37 ± 6.35	0.027
At proximal CS	3.20 ± 1.82	6.86 ± 6.06	0.022
At distal CS	3.84 ± 1.58	7.42 ± 5.83	< 0.01
Intracardiac spatial regularity			
SD of activation time difference from low RA to distal CS/ms	3.62 ± 2.01	4.99 ± 2.21	0.020

CL = atrial cycle length; ECG = electrocardiogram; RA = right atrial; SD = standard deviation; other abbreviations as in Table 1.

("rotor") of NIDAFL, because atrial timing remained "regular" by spectral analysis (Figs. 2A, 2B, and 5D to 5F). Although CL variability in NIDAFL has not previously been systematically studied, one preliminary study reported an elevated CL SD in NIDAFL (12.7 ms) versus IDAFL (5.8 ms) (12), and others have illustrated F-wave variability (4,11) and documented substantial intracardiac variability (5) in NIDAFL. Our study may underestimate the true variability in bi-atrial activation between groups, because activation of the anatomically complex LA may be less reproducible in NIDAFL than in IDAFL (8,17).

Possible bases for cycle variability in NIDAFL. F-waves reflect global atrial activation, and fluctuations may reflect variations in passive atrial activation including those due to varying functional block. In IDAFL, lower variability could result because the circuit is bounded more consistently anatomically (and less functionally) than many cases of NIDAFL (2). In IDAFL, macro–re-entry is constrained anteriorly by the TA (completely), posteriorly by anatomic and functional block in the crista terminalis (18) or functional block in sinus venosus-derived smooth RA (19), inferiorly by the eustachian ridge, and inferomedially by the CS ostium. Superiorly, functional block creates consistent turnarounds either anterior (2) or posterior (7) to the vena cava. Notably, passive activation of the remaining atria may also be "stabilized" in the RA by the large relative circuit size, and in the LA by consistent activation via coronary sinus musculature (CCW atrial flutter) or primarily via Bachmann's bundle (CW atrial flutter) (10).

Theoretically, atypical macro–re-entry may sustain wherever two conducting barriers and the inability of alternative paths to short circuit the primary wavefront occur (2,11). Thus, NIDAFL circuits are located at variable and possibly greater distances from anatomic obstacles than IDAFL, and their potentially small size (e.g., peri-atriotomy) may enable greater variability in passive atrial activation than in IDAFL. For example, stable (and entrainable) left atrial flutter circuits may be small and have been reported to result

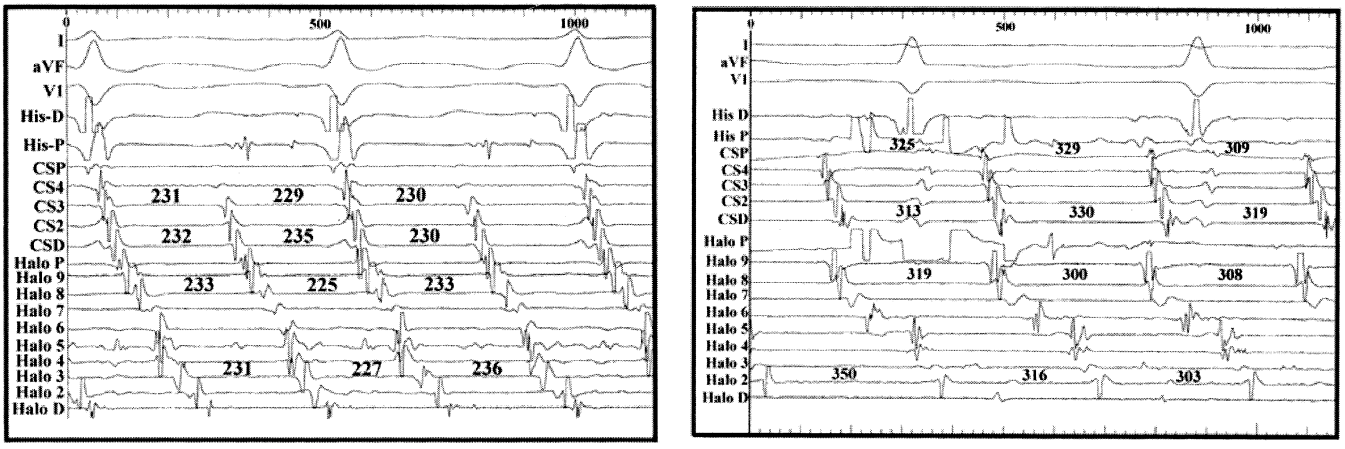

Figure 5. Intra-atrial variability in cycle length and activation sequence. **(A)** Counterclockwise isthmus-dependent atrial flutter (IDAFL) (patient in Figs. 2 and 4A) with mean cycle length (CL) 231 ms and standard deviation (SD): low lateral right atrium (RA) (Halo 3) 4.58 ms, septal RA (Halo 8) 4.37 ms, mid coronary sinus (CS3) 3.32 ms, and distal CS (CSD) 4.36 ms. Spatially, SD of activation time differences (CSD to Halo 3) was 3.32 ms. **(B)** Non–isthmus-dependent atrial flutter (NIDAFL) (patient in Figs. 3 and 4B). Mapping confirmed lateral RA re-entry with mean CL 303 ms and greater CL SD: low lateral RA (Halo 2) 6.23 ms, septal RA (Halo 8) 8.57 ms, proximal CS (CSP) 7.00 ms, and distal CS (CSD) 5.46 ms. Spatially, activation time (CSD to Halo 2) had SD 10.15 ms (Table 2).

in right atrial cycle-to-cycle variability ≥100 ms (5). Further studies on the sites and mechanisms of variability in IDAFL and NIDAFL are clearly required, and may help address the extent to which transitions to atrial fibrillation are determined anatomically or functionally.

Finally, it is necessary to show that our cases of NIDAFL do not represent variants of atrial fibrillation characterized by rapidly activating rotors (or foci) with fibrillatory conduction (18). First, sites of earliest activation (and adjacent isthmuses of slow conduction), identified from electroanatomic mapping, showed CL that were not short and conducted 1:1 to all atrial sites (Figs. 4D to 4G). Second, local electrograms at these sites did not show beat-to-beat changes in morphology seen in "type I" atrial fibrillation (20). Third, cases of NIDAFL were confirmed using concealed entrainment and thus do not represent "type II" atrial flutter (2), and their long CL (291 ± 42 ms; Table 1) are consistent with NIDAFL in structural heart disease (303 ± 78 ms in reference 5) rather than fibrillation. Fourth, cases were ablated successfully without atrial compartmentalization (at nonpulmonary venous sites). It is likely that future high-resolution mapping studies, in animal models and intraoperatively (18), will help further define the interface between macro–re-entrant NIDAFL and fibrillatory conduction (2).

Other explanations for greater wavefront variability in NIDAFL. Atrial wavefronts may also vary with ventricular or respiratory rates or autonomic tone. Ventricular systole modulates sinus CL through "ventriculophasic" mechanisms, but ventricular CL and A to V ratios were similar between IDAFL and NIDAFL (Table 1). Variable A to V ratios per se do not produce variable atrial loops (Fig. 4A), and variable loops were seen in NIDAFL even when A to V ratios were fixed (Figs. 4D and 4F). Although we did not record respiratory rates, breathing modulates atrial flutter CL (16), and this requires further study. Finally, there were no differences between groups in their incidence of diabetes mellitus (with possible dysautonomia), heart failure (enhancing sympathetic tone), or use of beta-blocking medications (Table 1).

Clinical significance. Electrocardiographic temporospatial phase analysis accurately separates NIDAFL from IDAFL and may help guide management. For example, in Figures 4E and 4F, quantitative ECG analysis correctly identified NIDAFL despite F waves resembling CCW-IDAFL. In Figure 4F, ECG analysis identified separate pre- and post-ablation mechanisms, guiding subsequent ablation. Furthermore, cycle-to-cycle variability of NIDAFL should be considered when interpreting post-pacing intervals during entrainment mapping and may contribute to the limitations of that technique in some studies (21).

Study limitations. We recorded cycle-to-cycle variability from a limited number of sites. Although we are currently extending our spatial resolution using noncontact mapping, artifactual variability from its smoothed endocardial geometry must be separated from actual cycle-to-cycle variations. Noise may affect ECG loops, although it is unlikely that noise would differ between groups, and our algorithm is quite resistant to noise (13). Furthermore, catheter noise may actually have been higher in IDAFL (with faster atrial and ventricular rates; Table 1), whereas bi-atrial activation was measured from stable low RA and CS electrodes.

CONCLUSIONS

Greater cycle-to-cycle variation in atrial activation timing and sequence characterize NIDAFL from CW and CCW IDAFL, allowing their robust separation from the ECG with sensitive temporospatial analyses. These results have implications for interpreting entrainment mapping and for guiding ablation and, mechanistically, support the concept that IDAFL and NIDAFL lie along a spectrum of intracardiac organization.

Acknowledgements

The authors thank Melvin Scheinman, MD, and Ronald Berger, MD, PhD, for their helpful comments on the manuscript. The authors also thank Nancy McCormick, RNP, and Kathleen Mills, BA, for help in coordinating these studies.

Reprint requests and correspondence: Dr. Sanjiv M. Narayan, Director, VA Electrophysiology Program, University of California, San Diego, Cardiology/111A, 3350 La Jolla Village Drive, San Diego, California 92161. E-mail: snarayan@ucsd.edu.

REFERENCES

1. Uno K, Kumagai K, Khrestian C, Waldo A. New insights regarding the atrial flutter reentrant circuit: studies in the canine sterile pericarditis model. Circulation 1999;100:1354–60.
2. Saoudi N, Cosio F, Waldo A, et al. Classification of atrial flutter and regular atrial tachycardia according to electrophysiologic mechanism and anatomic bases: a statement from a Joint Expert Group From the Working Group of Arrhythmias of the European Society of Cardiology and the North American Society of Pacing and Electrophysiology. J Cardiovasc Electrophysiol 2001;12:852–66.
3. Akar JG, Kok LC, Haines DE, DiMarco JP, Mounsey JP. Coexistence of type I atrial flutter and intra-atrial re-entrant tachycardia in patients with surgically corrected congenital heart disease. J Am Coll Cardiol 2001b;38:377–84.
4. Bochoeyer A, Yang Y, Cheng J, et al. Surface electrocardiographic characteristics of right and left atrial flutter. Circulation 2003;108:60–6.
5. Jais P, Shah DC, Haissaguerre M, et al. Mapping and ablation of left atrial flutters. Circulation 2000;101:2928–34.
6. Milliez P, Richardson AW, Obioha-Ngwu O, Zimetbaum PJ, Papageorgiou P, Josephson ME. Variable electrocardiographic characteristics of isthmus-dependent atrial flutter. J Am Coll Cardiol 2002;40:1125–32.
7. Schilling RJ, Peters NS, Goldberger J, Kadish AH, Davies DW. Characterization of the anatomy and conduction velocities of the human right atrial flutter circuit determined by noncontact mapping. J Am Coll Cardiol 2001;38:385–93.
8. Rodriguez L-M, Timmermans C, Nabar A, Hofstra L, Wellens HJJ. Biatrial activation in isthmus-dependent atrial flutter. Circulation 2001;104:2545–50.
9. Narayan SM, Feld GK, Hassankhani A, Bhargava V. Quantifying intra-cardiac organization of atrial arrhythmias using temporospatial phase of the electrocardiogram. J Cardiovasc Electrophysiol 2003b;14:971–81.

10. Marine JE, Korley VJ, Obioha-Ngwu O, et al. Different patterns of interatrial conduction in clockwise and counterclockwise atrial flutter. Circulation 2001;104:1153–7.
11. Kalman JM, Olgin JE, Saxon LA, Lee RJ, Scheinman MM, Lesh MD. Electrocardiographic and electrophysiologic characterization of atypical atrial flutter in man: use of activation and entrainment mapping and implications for catheter ablation. J Cardiovasc Electrophysiol 1997; 8:121–44.
12. Zhou L, John RM. Arial flutter cycle length variability on the surface ECG predicts non-isthmus dependent mechanisms (abstr). Circulation 1999;100:159.
13. Narayan SM, Bhargava V. Temporal and spatial phase analyses of the electrocardiogram stratifies intra-atrial and intra-ventricular organization. IEEE Trans Biomed Eng 2004d;51:1749–64.
14. Narayan SM, Smith JM. Exploiting rate hysteresis in repolarization alternans to optimize the sensitivity and specificity for ventricular tachycardia. J Am Coll Cardiol 2000c;35:1485–92.
15. Cain ME, Anderson JL, Arnsdorf MF, Mason JW, Scheinman MM, Waldo AL. Signal-averaged electrocardiography: ACC consensus document. J Am Coll Cardiol 1996a;27:238–49.
16. Stambler BS, Ellenbogen KA. Elucidating the mechanisms of atrial flutter cycle length variability using power spectral analysis techniques. Circulation 1996b;94:2515–25.
17. Ndrepepa G, Zrenner B, Weyerbrock S, Schneider MAE, Schmitt C. Activation patterns in the left atrium during counterclockwise and clockwise atrial flutter. J Cardiovasc Electrophysiol 2001;12:893–9.
18. Waldo A. Mechanisms of atrial flutter and atrial fibrillation: distinct entities or two sides of a coin? Cardiovasc Res 2002;54:217–29.
19. Friedman PA, Luria D, Fenton AM, et al. Global right atrial mapping of human atrial flutter: the presence of posteromedial (sinus venosa region) functional block and double potentials: a study in biplane fluoroscopy and intracardiac echocardiography. Circulation 2000;101: 1568–77.
20. Konings K, Smeets J, Penn O, Wellens H, Allessie M. Configuration of unipolar atrial electrograms during electrically induced atrial fibrillation in humans. Circulation 1997;95:1231–41.
21. Bogun F, Gender B, Li Y-G, Hohnloser SH. Ablation of atypical atrial flutter guided by the use of concealed entrainment in patients without prior cardiac surgery. J Cardiovasc Electrophysiol 2000;11: 136–45.